Carrier-density-wave transport property depth profilometry using spectroscopic photothermal radiometry of silicon wafers II: Experimental and computational aspects

Derrick Shaughnessy and Andreas Mandelis[a)]
Photothermal and Optoelectronic Diagnostics Laboratories, Department of Mechanical Engineering, University of Toronto, Toronto, Ontario M5S 3G8, Canada

(Received 9 October 2002; accepted 13 February 2003)

The experimental verification of a previously presented theoretical model for the photothermal radiometric (PTR) signal from an Si wafer excited by a laser of arbitrary wavelength is presented. A multiparameter fitting algorithm is developed and is used to fit experimental frequency scans to the theoretical model. The recombination lifetime and surface recombination velocity values extracted from the fits are consistent for all of the experiments performed. The diffusion coefficients for the more strongly absorbed excitation wavelengths are greater than those measured when using deeper penetrating excitation wavelengths. This discrepancy is discussed in terms of the dependence of the PTR signal on injected carrier densities and the nonlinearity of the PTR signal with temperature. The sensitivity of the PTR signal to a localized defect is shown to increase with the proximity of the defect to the centroid of the injected carrier density. The method amounts to carrier-density-wave depth profilometry of the relevant electronic transport parameters. © *2003 American Institute of Physics.* [DOI: 10.1063/1.1565491]

I. INTRODUCTION

Photothermal radiometry (PTR) relies on the collection of black body radiation from a sample that has been excited by optical radiation. A modulated source focused onto a silicon semiconductor sample will produce modulated temperature variations (thermal waves), due to rapid thermalization of carriers to the lowest state in the conduction or valence band, followed by Shockley–Read–Hall (SRH) recombination, as well as modulated excess free carrier densities (carrier density waves). Each of these perturbations results in a modulated infrared radiative emission that can be collected and used to uniquely determine the thermal and electronic transport properties of the sample: Carrier lifetime, τ, carrier diffusion coefficient (or diffusivity), D; front surface recombination velocity (FSRV); and back surface recombination velocity (BSRV).[1]

The effective carrier lifetime that is extracted using characterization techniques is an average of all of the carrier lifetimes in the sample:

$$\tau_{\text{eff}}^{-1}=\sum_i \tau_i^{-1}. \tag{1}$$

Since carrier lifetime in silicon is directly related to the defect density in the lattice structure, measuring the lifetime while varying the spatial distribution (i.e., depth) of the injected carriers should, in theory, allow for the creation of a spatial reconstruction of the defect density. The ability to create such lifetime depth profiles will be useful for separating the surface and bulk recombination lifetimes, as well as for monitoring impurity concentrations and ion implantation doses and depths.

The origins of the three-dimensional (3D) PTR signal and the theoretical framework required to model it using a source of arbitrary wavelength has been presented by the authors[2] and has been used to study the spectral dependencies of the PTR sensitivity to the carrier transport parameters. The purpose of the current work is to present experimental verification of the aforementioned model.

II. EXPERIMENTAL METHOD

The experimental PTR system for semiconductor metrology has been reported earlier.[3] The system has been modified to include a tunable titanium:sapphire (Ti:Sa) laser capable of operating over the wavelength range of 690–1100 nm whose emissions are monitored by a wavemeter with less than 0.1 nm resolution. An argon ion laser is used to pump the Ti:Sa laser or the Ti:Sa can be bypassed so that the Ar^+ emission can be focused directly on the sample to perform experiments with 514 nm excitation. The laser beam is modulated using an acousto-optic modulator and focused to a beam radius of approximately 80 μm on the sample. The IR emissions from the sample are collected by a pair of reflecting objectives and focused onto a nitrogen-cooled HgCdTe detector whose signal is demodulated using a lock-in amplifier (LIA). The data acquisition process is automated by a personal computer that is interfaced with the LIA and two stepper motors to control sample positioning.

The sample used for this investigation is a thermally oxidized, 675 μm thick, B^+-doped wafer with a resistivity between 20 Ωcm and 40 Ωcm, which corresponds to a doping level between 3.33×10^{14} cm^{-3} and 6.67×10^{14} cm^{-3}.[4]

[a)]Electronic mail: mandelis@mie.utoronto.ca

 © 2003 American Institute of Physics

Downloaded 18 Jul 2008 to 128.100.49.17. Redistribution subject to AIP license or copyright; see http://jap.aip.org/jap/copyright.jsp

TABLE I. Optical properties of Si for appropriate wavelengths.

λ (nm)	n Ref. 5	k Ref. 5	R	$\beta=\frac{4\pi k}{\lambda}$ (m^{-1})	$1/\beta$ (μm)
514	4.225	0.060	0.381	1.47×10^6	0.68
710	3.773	0.0115	0.338	2.04×10^5	4.91
810	3.685	0.006	0.328	9.31×10^4	10.74
950	3.6	0.002 26	0.32	3.0×10^4	33.4

One surface of the wafer was polished while the other was left bare. In order to avoid confusion when discussing the surface recombination velocities, since separate experiments are performed with excitation/collection on opposite sides of the wafer, the polished surface will be referred to as $z=0$ and the bare surface as $z=L$, and the respective surface recombination velocities as S_0 and S_L. Thus, when the polished surface is facing the excitation/collection optics, the FSRV will be designated as S_0 and the BSRV will be designated as S_L. Mechanical damage was introduced to a 5 mm×5 mm region of the bare surface using silicon carbide paper in order to produce a defect with a known spatial (depth) location.

All of the experiments were performed at room temperature in the open laboratory environment. A series of frequency scans were performed on the polished and bare surfaces of the wafer at four different wavelengths: 514 nm, 710 nm, 810 nm, and 950 nm, which correspond to absorption depths of 0.68 μm, 4.91 μm, 10.74 μm, and 33.4 μm, respectively (Table I).[5]

The experimental frequency response was normalized by the system response to a reference sample in order to remove any artifacts due to instrument transfer function variations over the chosen frequency range. The reference sample was a semi-infinite zirconium alloy with a known thermal diffusivity. The theoretical frequency response was calculated using the known beam size and used to calculate the instrumental transfer function. The amplitude transfer function is the ratio of the experimental amplitude to the theoretically predicted response and the amplitude of all subsequent experimental frequency scans was divided by this normalization factor before attempting theoretical fits. The transfer function for the phase is the difference between the experimental phase and the theoretically predicted response and this factor was subtracted from the phase of all subsequent experimental frequency scans.

III. MULTIPARAMETER FITTING ALGORITHM AND THEORETICAL FITS

Following normalization using the instrumental transfer function, the experimental frequency scans were fit to a theoretical model. The theoretical PTR response contains improper integrals with infinite upper limits and must be evaluated numerically.[2] Based on the physical quantity represented by the integrand, it is necessary that the integral approach a finite upper limit. This was verified through rigorous investigation of the dependence of the integrand on physically reasonable values of the electronic and thermal parameters. A MATLAB program was used to perform the integration numerically utilizing the built-in QUADL function.[6] The infinite upper limit was replaced by a finite upper limit that was chosen to ensure that any additional contribution due to a further increase in the upper limit was negligible. The value of this finite upper limit was verified and routinely reexamined to ensure that it was above the convergence limit of the integral in all cases. The program was then used to calculate a theoretical response for a given set of electronic and thermal parameters that were adjusted to best fit the experimental frequency scans using the following multiparameter fitting algorithm.

To begin the fitting, the following were used as seed values: $\tau=1$ ms, $D=20\ \mathrm{cm}^2/\mathrm{s}$, $S_0=300$ cm/s, $S_L=600$ cm/s, plasma weighting factor $C_p=1\times10^{-20}$ (arbitrary units), and thermal weighting factor $C_t=150$ (arbitrary units). The following steps were then followed to manipulate the parameter values until the theory fit the experimental results: (i) C_p and C_t were adjusted to match the magnitude and slope, respectively, of the low-frequency amplitude, (ii) the lifetime, τ, was adjusted to match the amplitude "knee" of the experimental response and step (i) was repeated since the change in lifetime shifts the position of the saturated region of the amplitude curve, (iii) the diffusion coefficient, D, was varied until the signal spread between the low- and high-frequency extremes of the phase was identical to the experimental response and step (i) was repeated to account for the shift of the amplitude curve, (iv) the FSRV was adjusted to reposition the amplitude knee and attempts were made to match the spread in the amplitude between the knee region and the high frequencies; step (i) was repeated to account for the shift of the amplitude curve, (v) the BSRV was adjusted to fit the midfrequency knee of the phase curve and the low-frequency amplitude without strongly affecting the other regions of the respective curves, and (vi) the procedure was repeated several times beginning with step (ii). The repetition of the aforementioned fitting algorithm is required to improve the fit in the frequency range most relevant to each parameter following the subsequent adjustment of the remaining parameters.

While attempts were made to maintain photoinjected carrier densities below the equilibrium majority carrier density in order to ensure that the transport parameter extracted from the fits would be those of the minority carriers, the PTR signal could not be resolved above the system noise at such low injection levels. The volume occupied by the injected carriers will vary with modulation frequency due to changes in the ac diffusion length $L_{\mathrm{ac}}=[D\tau/(1+i\omega\tau)]^{1/2}$. For $\omega\tau\ll1$, the beam radius and absorption depths are relatively small compared to L_{ac} allowing the excess carrier densities to be calculated under the assumption of a point source at the sample surface and the presence of carrier diffusion away from the photogeneration spot, using the following expression:

$$\rho_c=\frac{6P(1-R)(1-2e^{-1})}{\pi^2 h\nu D L_{\mathrm{ac}}}, \tag{2}$$

where P is the incident power, R is the reflectivity, $h\nu$ is the photon energy, and w is the Gaussian beam radius. At high

Downloaded 18 Jul 2008 to 128.100.49.17. Redistribution subject to AIP license or copyright; see http://jap.aip.org/jap/copyright.jsp

TABLE II. Calculated injected carrier densities for $f=10$ Hz [using Eq. (2)] and $f=100$ kHz [using Eq. (3)] assuming $D=15$ cm^2/s and $\tau=1$ ms.

λ (nm)	Excess carrier density, ρ_c, ($\times 10^{15}$ cm^{-3}) $f=10$ Hz; $L_{ac}=1.22$ mm	Excess carrier density, ρ_c, ($\times 10^{19}$ cm^{-3}) $f=100$ kHz; $L_{ac}=48.9$ μm
514	4.20	2.37
710	6.20	3.08
810	7.20	3.06
950	8.54	2.34

frequencies, the ac diffusion length is on the order of the beam diameter as well as the absorption depth of the longer wavelengths. At these frequencies, the excess carrier densities have been estimated by approximating the volume occupied by the excess carriers as the cylindrical absorption volume extended in all directions by the ac diffusion length resulting in the following expression:

$$\rho_c=\frac{P(1-R)\pi(1-1/e)^3\tau}{h\nu\left[\frac{\pi}{\beta}(w+L_{ac})^2+\pi w^2 L_{ac}+\frac{2}{3}\pi L_{ac}^3+\pi w L_{ac}^2\left(\frac{\pi}{2}-1\right)\right]}, \tag{3}$$

where β is the absorption coefficient of the excitation source in the sample. The ac diffusion lengths and the calculated excess carrier densities for modulation frequencies of 10 Hz, calculated using Eq. (2), and 100 kHz, calculated using Eq. (3), are presented in Table II assuming a lifetime of 1 ms and a diffusivity of 15 cm^2/s.

The calculated excess carrier densities assume that all recombination is occurring on the time scale of the SRH recombination lifetime. However, as the excess carrier density becomes greater than $\sim 10^{16}$ cm^{-3}, Auger recombination is superposed over the SRH recombination and becomes increasingly dominant as the concentration continues to increase. The Auger recombination lifetime can be calculated as:

$$\tau_p^{-1}=C_p p^2, \tag{4}$$

where $C_p \approx 0.9\times 10^{-32}$ cm^6 s^{-1}.[7] For the carrier densities calculated for 514 nm excitation, this results in Auger recombination lifetimes of 25.2 s and 198 ns for modulation frequencies of 10 Hz and 100 kHz, respectively. Thus, while Auger recombination will be irrelevant at low modulation frequencies, the increase in excess carrier density as the modulation frequency increases results in Auger recombination becoming the dominant process at high frequencies. For any carrier densities in excess of $\sim 10^{19}$ cm^{-3}, the short Auger lifetime results in a decrease of carrier densities that is essentially instantaneous on the time scale of the frequencies used in the current experiments and SRH recombination via lattice defects and impurities, and thus limits the carrier density to approximately 10^{19} cm^{-3}.[7,8] It should be noted, however, that inclusion of carrier diffusion away from the surface was found to maintain the apparent injection density below $\sim 10^{19}$ cm^{-3} (see Table II).

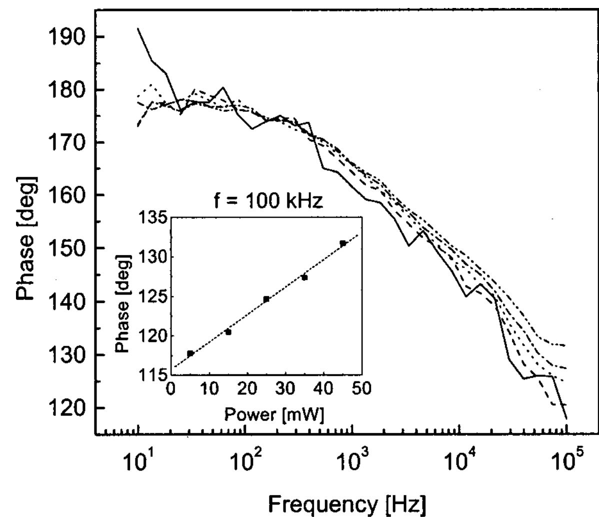

FIG. 1. PTR phase as a function of power for 514 nm excitation with carrier densities calculated using Eq. (3) at $f=100$ kHz (— 5 mW, $\rho_c=3.96\times 10^{18}$ cm^{-3}; -- 15 mW, $\rho_c=1.19\times 10^{19}$ cm^{-3}; ····· 25 mW, $\rho_c=1.98\times 10^{19}$ cm^{-3}; -·- 35 mW, $\rho_c=2.77\times 10^{19}$ cm^{-3}; and -·· 45 mW, $\rho_c=3.56\times 10^{19}$ cm^{-3}).

In order to determine the influence of any carrier–carrier interactions and other nonlinear effects on the PTR signal at the injection densities used for our experiments, frequency scans were performed for various incident powers on a wafer that was produced alongside the primary wafer used in this investigation. The amplitude response as a function of incident power appeared to be linear, although noise at low power may have masked any slight nonlinearities. However, the PTR phase (Fig. 1) showed a definite dependence on the power (i.e., injected carrier density) that became stronger with increased modulation frequency, which corresponds to an increasing carrier density. At 100 kHz, the phase lag decreases by approximately 15° as the calculated injected carrier density rises from 3.96×10^{18} cm^{-3} to 3.56×10^{19} cm^{-3}. This variation in phase with carrier density demonstrates a change in the carrier dynamics and recombination mechanisms that dominate the PTR signal. This range of carrier densities is well within the estimated range for the frequency scans performed at all four wavelengths and suggests that similar nonlinear effects were present, to varying degrees, during all of the frequency scans. Therefore, it is likely that Auger recombination is significant at the injection levels used in this investigation and the corresponding limitations of the photoinjected carrier densities are quite possible.

While there are no current presentations of the influence of nonlinear carrier dynamics on the PTR signal, there have been studies dealing with high injection levels in other photothermal techniques. Forget *et al.*[9] have presented the theoretical and experimental implications of the presence of Auger recombination at high pumping intensity on the relative weighting of the thermal and free carriers contributions to the photomodulated reflectance signal. A more complete theoretical approach to nonlinear recombination has been presented and experimentally validated by Wagner and Mandelis.[10,11] In addition to Auger recombination, surface

Downloaded 18 Jul 2008 to 128.100.49.17. Redistribution subject to AIP license or copyright; see http://jap.aip.org/jap/copyright.jsp

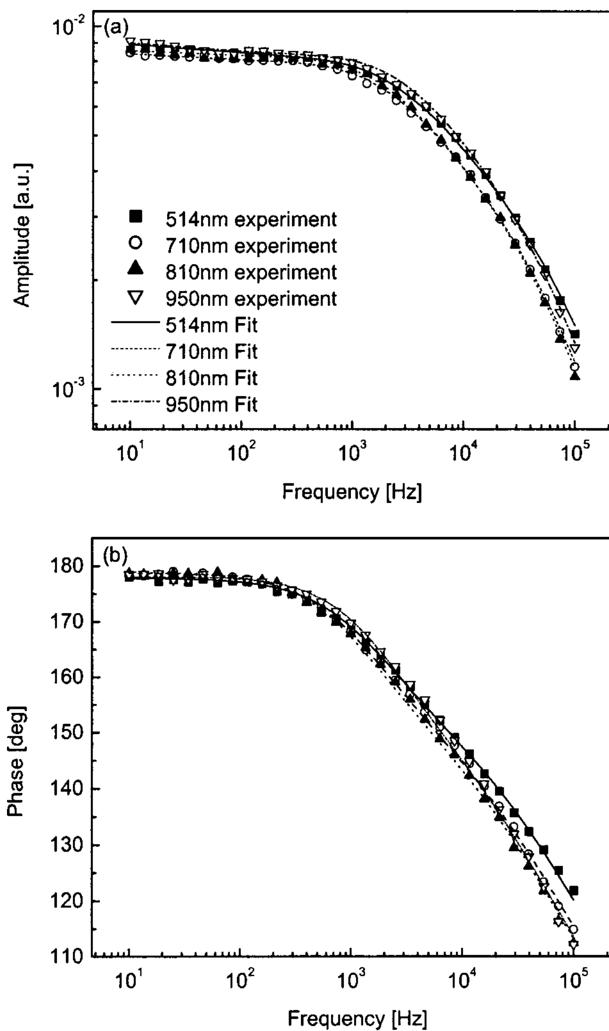

FIG. 2. Experimental frequency scans and theoretical fits for excitation/collection on the polished surface of the wafer.

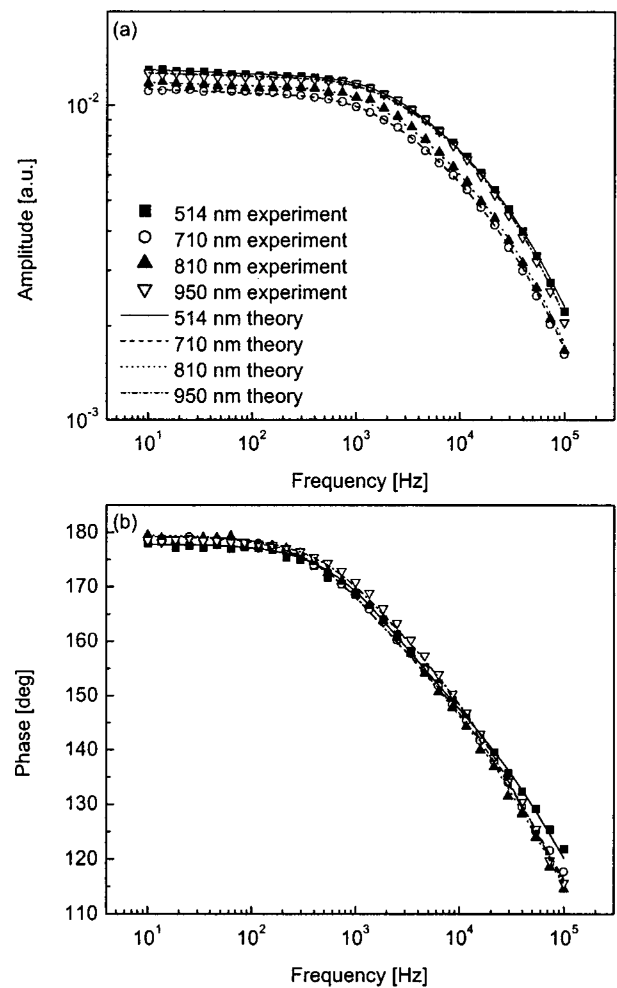

FIG. 3. Experimental frequency scans and theoretical fits for excitation/collection on the bare surface of the wafer.

band bending resulting from electric-field generation due to trapped carriers has also been discussed as a source of nonlinearities.[12] The physical phenomena responsible for the observed nonlinearities and their implications for the PTR signal will not be discussed in detail in this work but will be dealt with in a future study.

IV. EXPERIMENTAL RESULTS

The experimental frequency scans performed with excitation/detection on the polished surface in the intact region of the wafer and the corresponding theoretical fits are presented in Fig. 2. Error bars are not presented in Fig. 2 but are on the order of the symbol size for the lower frequencies and get smaller as the frequency increases. Since all of the experiments were performed at constant incident power, it was expected that the amplitude curves would increase in magnitude at all frequencies as the excitation wavelength is increased, assuming no significant variations in the carrier transport properties with depth. The decreasing photon energy results in an increase in the photon flux and thus, assuming no strong variation of quantum efficiency with wavelength, an increase in the PTR amplitude due to the greater number of electrons contributing to the depth integral.[2] This expected feature is not present for the amplitude curves presented in Fig. 2(a). The trend is present for the longer wavelengths but then reverses for the 710 nm and 514 nm scans so that the amplitude of the 514 nm is actually greater than that of the 950 nm scan at the high frequencies. The phase of the frequency scans for all wavelengths, with the exception of the 514 nm scan, have only slight differences. The phase lag of the 514 nm scan at high frequencies is much shorter than the other scans resulting in a smaller phase spread across the frequency range and a lower high-frequency slope.

The experimental frequency scans performed with excitation/detection on the bare (unpolished) surface in the intact region of the wafer and the corresponding theoretical fits, presented in Fig. 3, show similar trends in the PTR phase with respect to excitation wavelength. However, the amplitude curves [Fig. 3(a)] exhibit the separation discussed in the aforementioned paragraph for all but the 514 nm scan. The frequency scan with 514 nm excitation has a higher amplitude than expected and is similar in magnitude to that from the 950 nm scan. Again the error bars for these data points will be approximately equal to or smaller than the symbol size.

Downloaded 18 Jul 2008 to 128.100.49.17. Redistribution subject to AIP license or copyright; see http://jap.aip.org/jap/copyright.jsp

TABLE III. Results of fitting frequency scans to the theoretical model with excitation/collection incident on the polished surface of intact wafer.

λ (nm)	τ (ms)	D (cm^2/s)	FSRV S_0 (cm/s)	BSRV S_L (cm/s)	C_p ($\times 10^{-20}$)	C_t
514	1.00	23.50	120	400	1.560	260
710	1.00	17.00	110	400	0.780	260
810	1.00	14.10	100	400	0.592	210
950	0.95	15.00	230	500	0.625	295

The values of the electronic transport parameters resulting from the fits of the frequency scans on the intact wafer with the incident light and detector focused on the polished surface at $z=0$ are presented in Table III and for the incident light and detector focused on the bare surface at $z=L$ in Table IV. All of the theoretical fits, from both the polished and from the bare surface, yielded a lifetime of approximately 1 ms that has a relatively high uncertainty of approximately 100 μs due to the proximity of the saturation value for the PTR sensitivity to recombination lifetime. The surface recombination velocity for the polished surface, S_0, was between 100 cm/s and 230 cm/s for all fits, and the surface recombination velocity for the bare surface, S_L, was between 220 cm/s and 500 cm/s for all fits.

The values for the diffusion coefficients were not as consistent. Fitting the 514 nm frequency scan from the polished surface (FSRV$=S_0$) produced a much higher value (23.5 cm^2/s) than that of the other three frequency scans, which resulted in values of 17 cm^2/s, 14.1 cm^2/s, and 15 cm^2/s for the wavelengths 710 nm, 810 nm, and 950 nm, respectively. As expected for a higher diffusion coefficient, the spread in the phase is much smaller for the 514 nm scan than for the other three wavelengths, while the differences in the position of the phase knees are quite small [Fig. 2(b)]. Attempting to fit the phase with a lower value for the diffusion coefficient requires a much higher FSRV that decreases the amplitude spread preventing the amplitude from being fitted reasonably well. The fits to the frequency scans performed on the bare surface produced diffusivity values of 17.5 cm/s^2, 16.7 cm/s^2, 14.75 cm/s^2, and 15.0 cm/s^2 for excitations wavelengths of 514 nm, 710 nm, 810 nm, and 950 nm, respectively. These results compare well with those performed on the polished surface of the sample with the exception that the value from the 514 nm scan is not as far removed from the other results. The extracted diffusivities are all between the values for D_n ($\sim$35 cm^2/s) and D_p ($\sim$12.5 cm^2/s) found in a previous literature review.[1] Since a p-type wafer was used for the current investigation, under low-level injection, the

TABLE IV. Results of fitting frequency scans to the theoretical model with excitation/collection incident on the bare surface of intact wafer.

λ (nm)	τ (ms)	D (cm^2/s)	FSRV S_L (cm/s)	BSRV S_0 (cm/s)	C_p ($\times 10^{-20}$)	C_t
514	1.00	17.50	390	160	2.350	270
710	1.10	16.70	220	130	1.132	230
810	1.00	14.75	220	150	0.945	190
950	1.00	15.00	415	200	1.020	250

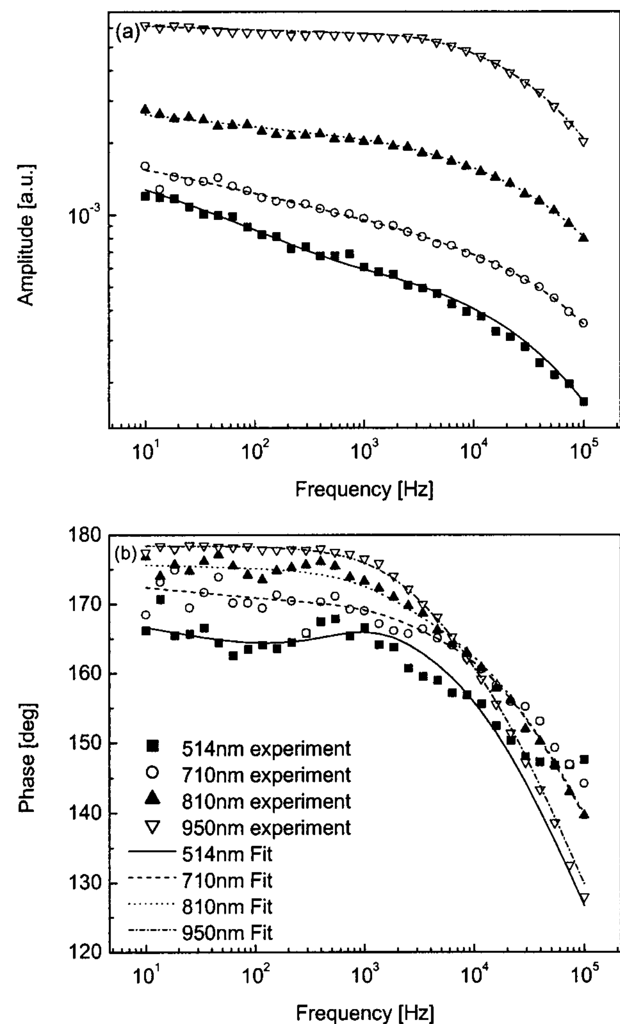

FIG. 4. Experimental frequency scans and theoretical fits for excitation/collection on the bare surface of the wafer and mechanical damage introduced to the front surface of the sample.

carrier diffusion would be controlled by the minority carriers so that the diffusivity values extracted from the fits would be expected to be $\sim$35 cm^2/s. However, since the photoinjected carrier densities were greater than the equilibrium majority carrier densities, the low-level approximation is not valid and, assuming that any energy released by photoexcited carriers and redistributed among the carrier-density wave does not raise the electron temperature enough to significantly increase the carrier diffusivity, an ambipolar diffusion coefficient intermediate to their individual rates is expected.

Frequency scans were also performed on the bare surface of the wafer with a mechanically damaged front surface (Fig. 4). Frequency scans performed using the strongly absorbed excitation sources (i.e., shorter wavelengths) are dominated by the signal from the thermal wave as evidenced by the nearly constant slope of the PTR amplitude. As the optical absorption depth of the incident radiation increases, the thermal-wave contribution, although still significant, is less dominant and the signal becomes characteristic of a carrier-density-wave signal as manifested by the amplitude knee at $\omega\tau\sim 1$. It is clear from Fig. 4(a) that as the wavelength of the excitation source decreases and more carriers

Downloaded 18 Jul 2008 to 128.100.49.17. Redistribution subject to AIP license or copyright; see http://jap.aip.org/jap/copyright.jsp

are deposited in the vicinity of the defect, the higher recombination rate of the defect area becomes more influential. The decreasing number of carriers in the carrier-density wave results in a lower PTR amplitude and an increase in the relative strength of the thermal-wave contribution with respect to that of the carrier-density wave. While fitting the high-frequency phase of the scans using the shorter excitation wavelengths was not possible due to the sensitivity to the inhomogeneous layer of damaged material at the surface, a fit of the 950 nm scan produced the electronic transport parameters: $\tau = 80\ \mu\text{s}$, $D = 12.5\ \text{cm}^2/\text{s}$, $S_1 = 10^5$ cm/s, and $S_2 = 220$ cm/s. These results are significantly different from the transport parameters for the intact region and are characteristic of poor-quality silicon (decreased lifetime and diffusivity, and increased FSRV.) Although it might be expected that the introduced defect would have no effect on bulk properties such as carrier recombination lifetime, it is very possible that the severity of the defect resulted in lattice damage well into the bulk of the sample thus creating or increasing the density of carrier recombination centers. While transport parameters could not be obtained for the damaged-layer data using shorter excitation wavelengths, the decrease of the carrier-density-wave contribution and the shift of the amplitude knee to higher frequencies both suggest that the carrier transport properties are more strongly affected by the near-surface defect as the optical absorption depth of the excitation source decreases. These results demonstrate that spectroscopic PTR can be used as a depth profilometric technique to monitor the depth dependence of photoexcited carrier lifetime and diffusion coefficient, as well as changes in the FSRV.

In order to investigate the question of uniqueness of fit and the tolerances of the extracted parameters, the front surface 514 nm excitation scan from the intact wafer was fit for various fixed values of FSRV. The amplitude and phase difference between the experiment and the theory are presented in Fig. 5 along with the standard deviation of each experimental data point. As the FSRV increased, it was necessary to increase the lifetime and decrease the diffusivity in order to maintain a reasonably good fit within the experimental error. As the diffusivity decreases, we see from Fig. 5(b) that the quality of the fit of the high-frequency phase decreases. An uncertainty of at most ~2–3 cm^2/s could be assigned for this diffusivity but the quality of the fit clearly decreases as this diffusivity falls below 22.5 cm^2/s. A similar examination of the 950 nm scan at the same position on the sample shows that the diffusivity can be no greater than ~15 cm^2/s, and the quality of the fit at the high-frequency phase decreases as the diffusivity is decreased in order to compensate for changes in the surface recombination values and the lifetime. Thus, while the diffusivity values for the 950 nm, the 810 nm, and, to a lesser extent, the 710 nm fits may vary only slightly when taking tolerances into account (since the quality of the fit is subjective depending on which portion of the frequency range is deemed more important), the diffusion coefficient from the scans with 514 nm excitation is definitely greater. Transverse surface scans performed at a fixed frequency for five frequencies in the usual range over a lateral distance of centimeters showed no drastic variations in the PTR signal that would support improper positioning of the wafer as a reason for the discrepancies in the diffusivities extracted from the fits.

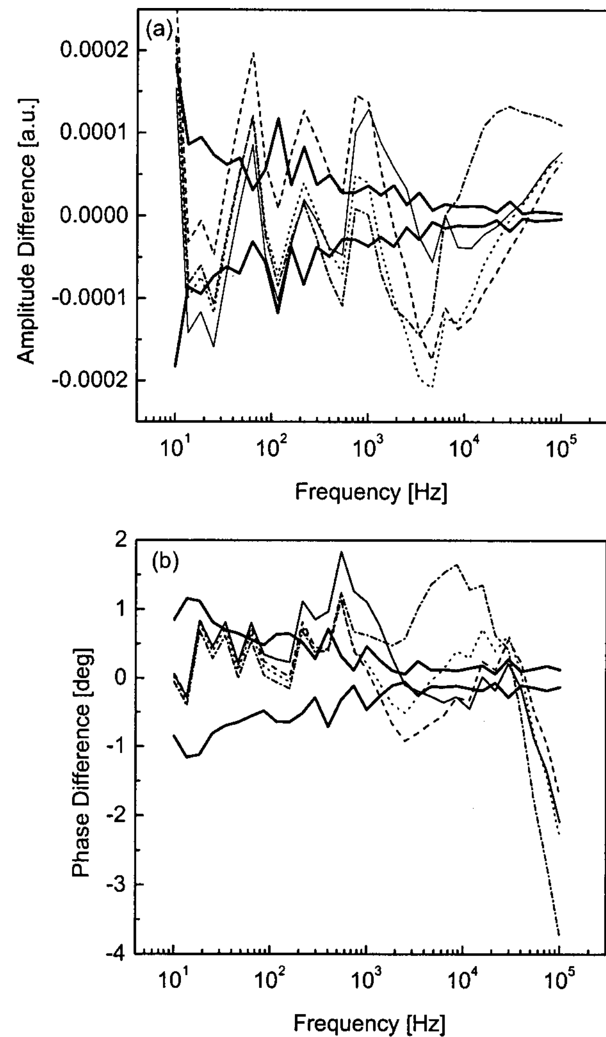

FIG. 5. Amplitude (a) and phase (b) difference between theoretical and 514 nm polished surface excitation experimental results for best fits using several fixed values of FSRV resulting in a range of diffusivity values (— experimental error; — $\tau = 0.30$ ms, $D = 25.0\ \text{cm}^2/\text{s}$, $S_0 = 0$ m/s, $S_L = 600$ cm/s; -- $\tau = 1.0$ ms, $D = 23.5\ \text{cm}^2/\text{s}$, $S_0 = 150$ cm/s, $S_L = 300$ cm/s; ····· $\tau = 2.0$ ms, $D = 22.5\ \text{cm}^2/\text{s}$, $S_0 = 210$ cm/s, $S_L = 300$ cm/s; and -·- $\tau = 2.0$ ms, $D = 17.0\ \text{cm}^2/\text{s}$, $S_0 = 500$ m/s, $S_L = 100$ cm/s).

Although, as discussed in Sec. III, Auger recombination is expected to be a significant factor at high modulation frequencies, it is not likely that this recombination process is directly responsible for the higher diffusion coefficients at shorter wavelengths because the excess carrier densities at the higher modulation frequencies are nearly identical. However, the energy released to the lattice by the hot carriers produced during Auger recombination is a thermal source whose spatial and temporal distribution is not accounted for in the theory. This thermal energy will be deposited in a volume that decreases with wavelength and is much smaller than that assumed in the preceding section since diffusion on the time scale of the Auger recombination lifetime will be small compared to the distances travelled by carriers recombining via SRH mechanisms. This effect would result in a higher effective diffusion coefficient in the present model.

Downloaded 18 Jul 2008 to 128.100.49.17. Redistribution subject to AIP license or copyright; see http://jap.aip.org/jap/copyright.jsp

Additionally, the shorter wavelengths have more energetic photons that result in more energy being released to the lattice during the rapid (~ps) thermalization process following optical excitation. The PTR amplitude is proportional to $\sigma\varepsilon(T^4\text{-}T_o^4)$, where σ is the Stefan–Boltzmann constant, ε is the effusivity, and T_o is the ambient temperature, and therefore is nonlinear in T. The departure of the diffusion coefficient values for the very strongly absorbed 514 nm scans from the values found at longer wavelengths (i.e., deeper absorption depths) using a linear model may also be due to a thermal nonlinearity arising from the confinement of the energy released in the sample to the very near surface.

V. CONCLUSION

A multiparameter algorithm for fitting the previously presented 3D model for the PTR signal from an indirect gap semiconductor excited by light of arbitrary wavelength[2] has been presented and used in depth profilometric measurements to fit experimental frequency scans performed using strongly absorbed and deeper penetrating excitation sources. The transport parameters, with the exception of the carrier diffusivity, extracted from the fits are similar for each wavelength in intact Si attesting to the uniform electronic environment inside the bulk of the silicon sample and to the satisfactory reliability of the multiparameter fitting technique. Nonlinearities of the PTR signal with temperature have been considered to explain the discrepancies between the carrier diffusivities obtained from wavelength-scanned carrier-density-wave depth profilometry. The depth profilometric potential of spectroscopic PTR was demonstrated using a surface-damaged silicon wafer and performing frequency scans at several excitation wavelengths/optical absorption depths.

ACKNOWLEDGMENTS

The authors are grateful to the Natural Sciences and Engineering Research Council of Canada (NSERC) for a Research Grant (for one of the authors A.M.) and to Materials and Manufacturing Ontario (MMO) for an Enabling Research Contract.

[1] M. Rodriguez, A. Mandelis, G. Pan, L. Nicolaides, J. A. Garcia, and Y. Riopel, J. Electrochem. Soc. **147**, 687 (2000).
[2] D. Shaughnessy and A. Mandelis, J. Appl. Phys. **93**, 5236 (2003).
[3] M. Rodriguez, A. Mandelis, G. Pan, J. A. Garcia, V. Gorodokin, and Y. Raskin, J. Appl. Phys. **87**, 8113 (2000).
[4] ASTM F723-99 (ASTM International, West Conshohocken, PA, 1999).
[5] D. F. Edwards, in *Handbook of Optical Constants of Solids*, edited by E. D. Palik (Academic, New York, 1998).
[6] MATLAB version 5.2, The Mathworks, Inc. (1998).
[7] L. Passari and E. Susi, J. Appl. Phys. **54**, 3935 (1983).
[8] E. J. Yoffa, Phys. Rev. B **21**, 2415 (1980).
[9] B. C. Forget, D. Fournier, and V. E. Gusev, Appl. Phys. Lett. **61**, 2341 (1992).
[10] R. E. Wagner and A. Mandelis, Semicond. Sci. Technol. **11**, 289 (1996).
[11] R. E. Wagner and A. Mandelis, Semicond. Sci. Technol. **11**, 300 (1996).
[12] Y.-S. Lu, S.-Y. Zhang, and Z.-L. Qian, J. Appl. Phys. **74**, 4710 (1993).

Downloaded 18 Jul 2008 to 128.100.49.17. Redistribution subject to AIP license or copyright; see http://jap.aip.org/jap/copyright.jsp